# Construction and Demonstration of Access Link for Millimeter Wave UAV Base Station Network

Ryunosuke MASAOKA(1) Gia Khanh TRAN(1),
(1) Department of Electronic Engineering, Tokyo Institute of Technology 2-12-1 Ookayama, Meguro-ku, Tokyo, 152-8550 Japan
E-mail1: {masaoka, khanhtg}@mobile.ee.titech.ac.jp

***Abstract:*** In today's society, wireless communications are available anytime, anywhere. However, there are times when communication may become unavailable. This is when access is concentrated during a large-scale event, a major disaster, or when a base station goes out of service. Therefore, constructing a temporary network that can provide high-capacity communications and flexibly change its service location is being considered. In this paper, we examine the feasibility of combining UAVs, which can be remotely operated and flown unmanned regardless of ground conditions, with a millimeter wave signaling system that can achieve high-speed transmission.

***Keywords:*** ***UAV, IEEE802.11ad, Millimeter wave, Experiment***

## 1. Introduction

In today's society, it is clear that telecommunications is an indispensable technology for daily life. The number of subscriptions in Japan for mobile communications, including cell phones, which we carry and use all the time, was huge, e.g. approximately 254 million devices at the end of September 2022, an increase of 3.5% over the previous year [1]. In addition, Japan's average traffic per subscription in December 2022 has increased by about 1.6 times in three years and 1.2 times in one year [2]. While high-quality communication is available to everyone, there are situations where communication becomes disabled. For example, the 6.5-magnitude Kumamoto earthquake in April 2016 caused landslides and commercial power outages that knocked out as many as 400 cell phone base stations, temporarily disabling cell phone services [3]. During large-scale events, the number of accesses and the amount of traffic in a local area increases due to the active posting of videos and photos due to the widespread use of SNS, creating a situation where sufficient communication was impossible. Adding more base stations to cope with these temporary situations is costly for installation and maintenance. Therefore, there is a need for a temporary network that can provide high-capacity communications and can change its location flexibly. In this paper, we will use UAV base stations that utilize millimeter wave band radio waves to address these issues. Millimeter wave band radio waves are in the 30-300 GHz band, a high-frequency band characterized by high-capacity, low-latency communications. In addition, UAVs are not dependent on the ground environment, such as traffic conditions, and can be deployed remotely and unmanned. Although network construction utilizing UAV base stations has been considered previously, narrow-band microwaves had been used [4].

In this paper, we examine the construction of a UAV base station network using wide-band millimeter-wave and demonstrate its usefulness through empirical experiments and theoretical studies.

## 2. Millimeter Wavee UAV Base Station

### 2.1. Overall Architecture

The system architecture of a millimeter wave UAV base station is shown in Figure 1 [5]. Here, we consider a situation where the existing cellular communication network is no longer available. The entire system is divided into two parts: backhaul UAVs and access link UAVs. The backhaul UAVs connect the access link UAVs with available ground base stations far from the user. By deploying an appropriate location and number of backhaul UAVs, multi-hop communication is possible even when the distance between the user and the ground base station is apart. Access link UAVs communicate directly with users instead of base stations. Millimeter waves are used for all radio communications among these backhaul UAVs and access UAVs, that can guarantee wideband communications. On the other hand, these bands are almost not disfracted and are greatly attenuated by obstructions. Such disadvantages can be alleviated by employing. UAVs in our architecture, since UAVs can provide good communication channel via beam-forming technique in the upper airspace area with good visibility not being affected by obstructions. In addition, since there has been little use of communications in the sky area, the band is also beneficial from interference-free communication environments.

In the future, satellite communications such as “Starlink” and UAV-based communication technologies such as HAPS are expected to be used for communication from the sky. The UAVs in this architecture will be used at altitudes of tens to hundreds of meters, so the communication distance will be relatively short. As a result, the loss will be smaller than other technologies, and communication will be possible with low latency [6][7].

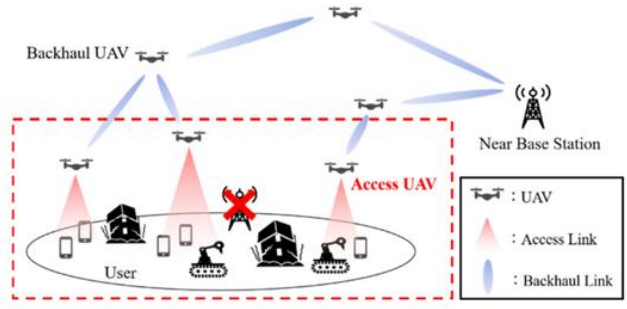


**Figure 1: Overall Architecture [5]**

### 2.2. Millimeter Wave Wireless Communication Technology

Millimeter waves are radio waves with a frequency range of 30~300 GHz [8]. In this research, we utilize the 60 GHz band, which is a license-free band and can be easily implemented [9].

Radio waves in the 60 GHz band are used for motion sensors and radar with high-precision positioning functions, as well as IEEE802.11ad/ay. This data communication standard utilizes the 60 GHz band [8]. In addition, this research utilizes IEEE802.11ad communication standard devices.

This is a brief introduction to IEEE 802.11ad. The basic specifications of IEEE 802.11ad are shown in Table 1. In addition, IEEE802.11ad has a function to adjust beamforming according to the procedure shown in Figure 2 [10]. This determines the beam direction and improves directivity.

Table 1: Specification IEEE802.11ad ( WiGig )

| | |
|---|---|
| Frequency Band | 60GHz |
| Max Antenna Power (JP) | 24dBm |
| Max Antenna Gain (JP) | 47dBi |
| Number of Channels (JP) | 4 |
| Channel Width | 2.16GHz |
| Modulation Method | SC / OFDM |

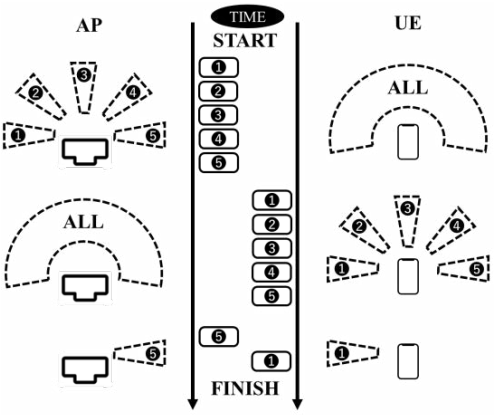


Figure 2: Beamforming Procedure

### 2.3. UAV Technology

In today's society, wireless communications are available anytime, anywhere. However, there are times when connectivities may become unavailable. This is when access is concentrated during a large-scale event, a significant disaster, or when a base station goes out of service. Adding more base stations to cope with such temporary situations is costly for installation and maintenance. Therefore, constructing a temporary network that can provide high-capacity communications and flexibly change its service location is being considered. In this paper, we examine the feasibility of combining UAVs, which can be remotely operated and fly in an unmanned manner regardless of traffic and other ground conditions, together with a millimeter-wave data channel that can provide high-speed transmission. We demonstrate its usefulness through demonstration experiments and theoretical studies.

## 3. Experimental Device

### 3.1. Millimeter Wave Communication Device

Table 2: Anntena Specification

| | |
|---|---|
| Size | 210mm×115mm×95mm |
| Weight | 0.87kg |
| Wireless Chip | Wireless-AC 17265 |
| Wireless Standard | IEEE802.11ad |
| Array Antenna | 10041R |
| Power Supply | 65W |
| Max MCS | 12 |
| Max Transmission Speed | 4.620Gbps |
| Antenna Gain [11] | 25.4dBi |
| Scan Angle (deg.) [11] | ±13.5 |

Table 2 shows the millimeter wave devices' performance in the demonstration experiment. The reasons for selecting this device were that it is small and light-weighted enough to be mounted on a UAV and is capable of 100-meter communications. The device comprises a small PC, an array, and a lens antenna [11].

### 3.2. UAV

The demonstration experiment used two "Matrice 600 Pro" UAVs manufactured by DJI. They can carry a maximum of 6 kg of load, and their performance is shown in Table 3 [12].

Table 3: Matrice 600 Pro Specification

| | |
|---|---|
| Size | 1668mm×1518mm×727mm |
| Weight | 9.5kg |
| Max Takeoff Weight | 15.5kg |
| Hovering Time | 32min |
| Battery Capacity | 4500mAh |
| Battery Voltage | 22.2V |
| Number of Batteries | 6 |

## 4. Experiments and Discussion

The following 3 experiments were conducted using the devices described in Section 3 [10].

+"4.1. Direct Experiment"

This experiment examined changes in throughput by varying the height of the UAV against the fixed ground user.

+"4.2. Coverage Measurement"

This experiment varied the ground user's location against a UAV base station hovering at a certain height to measure its coverage.

+"4.3. Ground Reflection Experiment"

When there are 2 UAV base stations, this experiment investigated how much ground reflection affects the communications.

A professional pilot was asked to manage and operate the UAVs in the demonstration experiment. The experiment was conducted in a rural area with little pedestrian traffic, such that the UAVs could be safely operated. In addition, throughput was used to evaluate the quality of communications. The flight time of the UAV used in the experiment was about 20 minutes per flight, prioritizing safety. Therefore, it was only possible to acquire experimental data from limited scenarios. The millimeter wave wireless communication device was equipped with Ubuntu, and throughputs were measured using the iperf3 command. The measured values were evaluated at MAC layer.

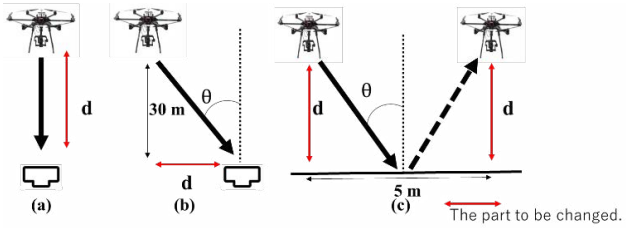


Figure 3: Diagram of Experiment Scenarios

Figure 4: UAV with Millimeter Wave Device

**Figure 5: Experimental Field**

### 4.1. Direct Experiment

Experiment

A schematic diagram of the experiment is shown in Figure 3(a). The UAV equipped with millimeter wave interfaces and the experimental field are shown in Figures 4 and 5 respectively. The relationship between UAV-UE vertical distance and throughput was investigated. Throughput measurements were taken by increasing the altitude of the UAV by each 5m step. The measurement results are shown by dots in Figure 6.

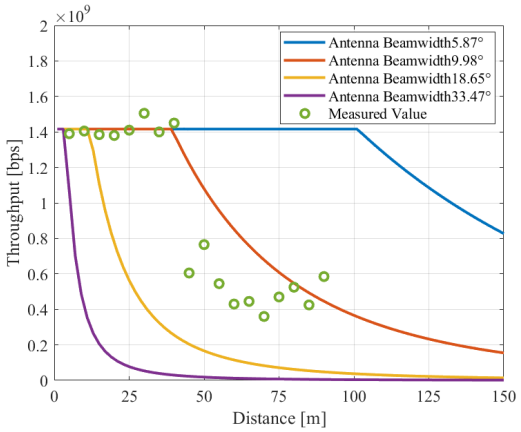


**Figure 6: Results of the Direct Experiment**

Comparison with theoretical analysis and discussion

From Frith's transmission equation, the received power $P_r$ is calculated in free space by Eq.(1) where $\lambda$ is the wavelength, $d$ is the distance, $G_t$ is the transmit antenna gain, $G_r$ is the receive antenna gain, and $P_t$ is the transmit power [13]. $L_{ox}$ is the atmosphere attenuation due to oxygen, at the amount of 16dB per km for the considered 60GHz band [14].

$$P_r = 20\,log\left(\frac{\lambda}{4\pi d}\right) + G_t + G_r + P_t - L_{ox} \quad [dB] \qquad (1)$$

The Shannon's communication capacity is calculated by Eq.(2) where $B$ is the bandwidth and SNR is the ratio of a received signal $P_r$ to noise power $P_n$ [15].

$$C = Blog_2(1 + \text{SNR}) \quad [bps] \qquad (2)$$

Shannon capacity is the value of the theoretical limit of communication capacity. Since the theoretical maximum communication rate of the devices used in the demonstration experiment is $C_0 = 4.620$ Gbps, the theoretical throughput, in this case, can be calculated by Eq.(3) [10].

$$T = \alpha \times min\,(C_0, C) \quad [bps] \qquad (3)$$

Where α is a spectral efficiency coefficient due to loss of specific communication protocol (e.g. MAC portion over the whole physical frame, bandwidth and time usage efficiency, etc.). In this paper, α is estimated from the difference between the saturated throughput of the experiment and theoretical results. The result was $\alpha = 1/3.2636$. The parameter values utilized in the simulation are listed in Table 4.

**Table 4: Simulation Parameters**

| | |
|---|---|
| **Frequency Band** | 60GHz |
| **Transmission Power** | 15dBm |
| **Noise Figure** | 10dB |
| **Bandwidth** | 1.88GHz |
| **Max Antenna Gain** | 25.4dBi |
| **Scan Angle (deg.) [11]** | ±13.5 |

The transmit spectrum conforms to the spectrum mask shown in Figure 7 [16]. The bandwidth is 2.16 GHz, but not all of it can be used for communication because of the guard bands. In this paper, 1.88 GHz is considered as the bandwidth [16]. For antenna gain, we use the antenna model in [17]. Based on this model, as the peak of the antenna gain is 25.4dBi we found that antenna beamwidth corresponds to 9.98deg. Simulations were performed by assuming that the operation to optimize the antenna gain by adjusting the beamforming was performed on both the transmitting and receiving antennas.

The results of the theoretical simulation are shown by solid lines in Figure 6. For comparison, we also performed theoretical simulations with antenna gains of 15, 20, and 30dBi. The corresponding beam widths are 33.47deg, 18.65deg and 5.87deg respectively. From these results, the received power decreases as the distance increases, and thus the SNR deteriorates. Therefore, it can be seen that the channel capacity also decreases, resulting in smaller throughput. Simulations using Eq.(3) show a similar distribution trend. We also consider that 5~40m takes almost the same value for throughput and the maximum value. We assume the UAV barely communicates at a distance due to the degraded SNR.

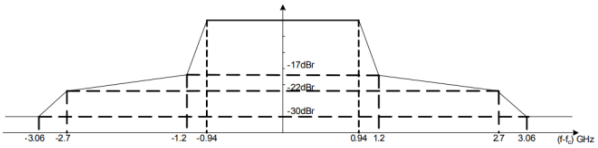


**Figure 7: Transmit spectrum mask[16]**

### 4.2. Coverage Measurement

Experiment

A schematic diagram of the experiment is shown in Figure 3(b). Coverage was measured by varying the position of the ground user against a fixed-height UAV. This time, the altitude of the UAV was set at 30m, and UE's locations were set apart by each 2.5m step from the center beneath the UAV. Dots in Figure 8 shows the measurement results.

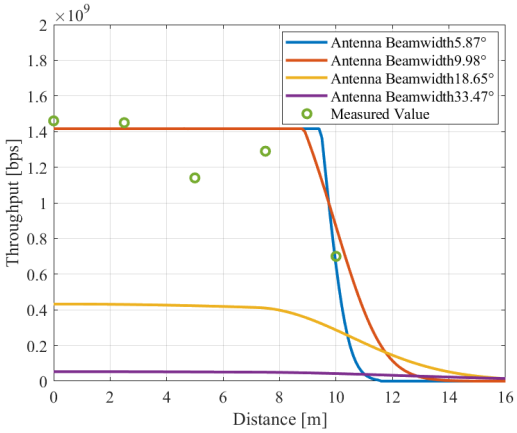


**Figure 8: Results of Coverage Measurement**

Comparison with theoretical analysis and discussion

The longest straight line distance is approximately 31.6m ($\approx \sqrt{30^2 + 10^2}$), so the maximum value for the device utilized in the demonstration experiment should be obtained from "4.1. Direct Experiment". However, as the distance increased, the alignment between the UE and the main lobe of the UAV's downward beam was worsen, which yielded directivity losses. Therefore, the antenna gain and the received power were reduced, resulting in lower throughput.

The results of the theoretical simulation are shown in Figure 8, which reveals similar performance trend between theoretical and experimental results. Furthermore, owing to the beam steering capability of the antenna upto ±13.5deg, the antenna coverage can be extended to a ground radius of 7.5m, which corresponds to an antenna angle of roughly 14deg ($\approx arctan\,(7.5/30)$).

### 4.3. Ground Reflection Experiment

Experiment

A schematic diagram of the experiment is shown in Figure 3(c). The experiment was to observe how ground reflections affect the communications of UAV base stations under conditions of two closely located UAVs. In this experiment, one of the UAV worked as a base station while the other played the role of a UE. Here, the interference was evaluated by the quality of the indirect communication link via ground reflection path between the two hovering UAVs. In other words, the higher throughput achieves, the stronger signal via the reflected path arrives at the other UAV. In the measurements, the horizontal distance between the UAVs was set to 5m and the throughputs were measured when both UAVs increased their altitudes gradually. The snapshot of the experiment can be seen in Figure 9. The measurement results are shown by dots in Figure 10.

**Figure 9: Experimental Observations of Ground Reflection**

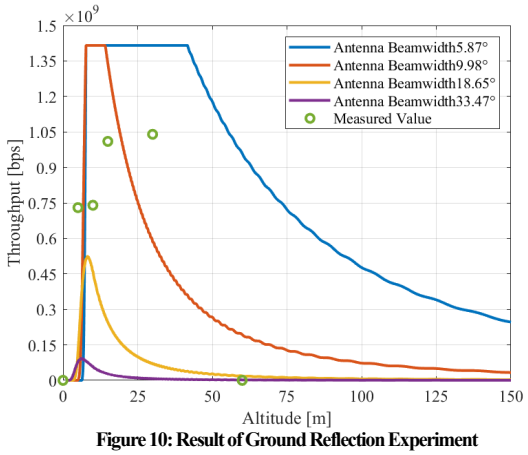


**Figure 10: Result of Ground Reflection Experiment**

Comparison with theoretical analysis and discussion

The observed throughput indicates the existence of ground reflection. Communication was disabled at an altitude of 0m because there was no radio-wave path available between the transceiver pair. The gradual increase in throughput at higher altitudes can be attributed to the improvement in directivity of the reflected path, as the incident angle becomes smaller. This agreed with the results measured in Sect. 4.2. After reaching the maximum throughput value at around the altitude of 30m, the curve again decreased until no throughput could be measured at the altitude of 60m. This can be explained by the longer distance of the reflected path (approximately 120m, which is double of the altitude 60m) that contributes to the degradation of SNR.

Similar trend can be observed in our numerical analysis result. The simulation employs a two-wave model to account for ground reflections [18]. There was some grass growing on the ground where the demonstration experiment was conducted, so the parameters were set assuming wet ground [18]. The simulation results are also shown in the same figure, which showed that the distribution is slightly different, but it rises as the altitude increases up to a certain point, and then decreases. The reason why the measured values differ from the simulated values is that the conductivity and dielectric constant values differ due to different ground environments and that the shape of the ground is not in an ideal state in the real experiment. Furthermore, we performed simulations with an antenna gain of 25.4dBi and different ground materials to confirm their effects [18][19]. The results are shown in Figure 11, and the measured values' trends did not follow exactly any specific materials, even for metals that are conductors. Therefore, it is possible that one of the main reasons for this discrepancy is due to the influence of the ground shape, which is not perfectly flat as assumed in our numerical analysis.

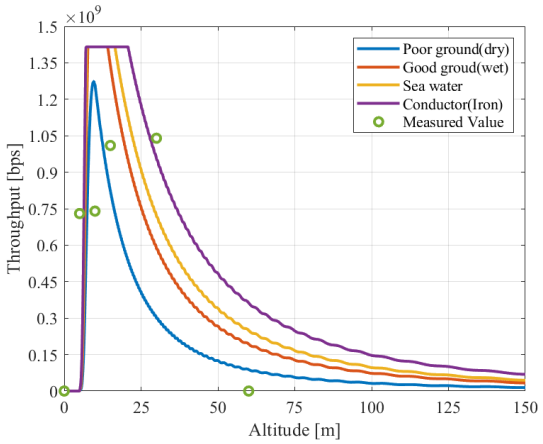


**Figure 11: Ground Reflection Experiment for Various Materials**

## 5. Summary

In this paper, we investigated the coverage of millimeter wave UAV base stations and the effect of ground reflection on the coverage of UAV base stations to establish a temporary network area in the event of a disaster or other communications outage through demonstration experiments and theoretical investigations.

It was found that a high-capacity communication of approximately 1.5 Gbps was possible using IEEE802.11ad on the experimental device. It was also confirmed that interference waves were generated by ground reflection. Furthermore, good matching between the two evaluation results validated the reliability of our measurement results, and the constructed theoretical model can be used for future model-based investigation for system design.

## 6. Acknowledgment

We would like to express our sincere gratitude to all the individuals and organizations that have contributed to the publication of this work. We are also grateful to the Telecommunications Advancement Foundation and the Ministry of Internal Affairs and Communications' SCOPE program JP235003015, for providing financial supports for this research. Especially, we would like to thank Mr. Tomoki Morioka, who helped to conduct the experiments.

## 7. Reference

[1] Ministry of Internal Affairs and Communications," Announcement of Quarterly Data on the Number of Telecommunications Service Contracts and Market Share (FY2022 Q2 (End of September))"2022.

[2] Ministry of Internal Affairs and Communications," Current Status of Mobile Communication Traffic (December 2022)" 2022 (in Japanese).

[3] Ministry of Internal Affairs and Communications," Survey Results on Ideal State of Information and Communications in Kumamoto Earthquake", 2017.

[4] Antonio Guillen-Perez, "Flying Ad Hoc Networks: A New Domain for Network Communications", Sensors 2018, 18(10), 3571, 2018.

[5] Gia Khanh Tran, Masanori Ozasa, Jin Nakazato. NFV/SDN as an Enabler for Dynamic Placement Method of mmWave Embedded UAV Access Base Stations, MDPI Network, Sept. 2022.

[6] Ohishi," Impacts by Mega-Constellations to Astronomical Observations", The astronomical herald 113(3), 2020.

[7] Ozasa,"A Study on Design of Millimeter Wave Band UAV Base Stations for Access", Master Thesis 2022 (in Japanese).

[8] Kazuaki Takahashi," Industrial Trends and Future View of Millimeter Wave Wireless Technology Using IEEE802.11ad/WiGig", The Journal of IEICE (in Japanese).

[9] Ministry of Internal Affairs and Communications," Technical Requirements for Diversification of 60 GHz Band Radio Equipment", 2019.

[10] Morioka," Construction of Experimental System for Mm-Wave UAV Base Station" IEICE Technical Report, 2022 (in Japanese).

[11] Adam Chin, "Simulation Report for Planar Lens & RFEM (2-by-8)", intel, 2018.

[12] DJI,"DJI Matrice 600 Pro", https://www.dji.com/jp/matrice600-pro.

[13] Karasawa,"Fris-Formula", Technical Report YK-040, 2020 (in Japanese).

[14] Adel Barakat, "Improved gain 60GHz CMOS antenna with N-well grid", IEICE Electronics Express, Vol. 13, No.5, 1-6, 2016.

[15] C.E.SHANNON,"A Mathematical Theory of Communication", Reprinted with corrections from The Bell System Technical Journal, Vol.27,pp.379–423,623–656, 1948.

[16] "IEEE Standard for Information technology--Telecommunications and information exchange between systems--Local and metropolitan area networks--Specific requirements-Part 11: Wireless LAN Medium Access Control (MAC) and Physical Layer (PHY) Specifications Amendment 3: Enhancements for Very High Throughput in the 60 GHz Band," in IEEE Std 802.11ad-2012 (Amendment to IEEE Std 802.11-2012, as amended by IEEE Std 802.11ae-2012 and IEEE Std 802.11aa-2012) , vol., no., pp.1-628, 28 Dec. 2012.

[17] I. Toyoda, M. Ando, K. Iigusa, H. Sawada, T. Seki, S. Nishi, S. Kitazawa, A. Miura, Y. Fujita, H. Uchimura, and Y. Hirachi, "Mathematical Antenna Model with a Rotationally Symmetric Beam for System Design of Wireless Personal Area Networks," IEICE Trans. Commun. (Japanese Edition), Vol. J93-B, No. 5, pp. 781–790, May 2010 (in Japanese).

[18] J.D.Parsons , "The Mobile Radio Propagation Channel. Second Edition", John Wiley & Sons Ltd, 2000.

[19] Chen, Dong & Yen, Max & Lin, Paul & Groff, Steve & Lampo, Richard & Mcinerney, Michael & Ryan, Jeffrey, "A Corrosion Sensor for Monitoring the Early-Stage Environmental Corrosion of A36 Carbon Steel. Materials", 2014.